Nanoscale

Accepted Manuscript

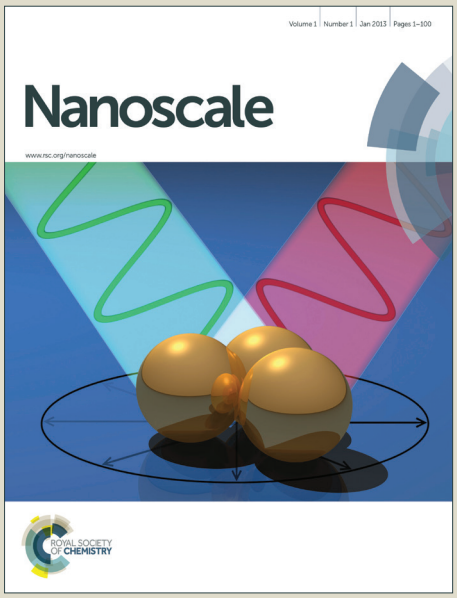

Growth of wafer-scale MoS_2 monolayer by magnetron sputtering

Junguang Tao,[a, c,] Jianwei Chai,[a,*] Xin Lu,[b] Lai Mun Wong,[a] Ten It Wong,[a] Jisheng Pan,[a] Qihua Xiong[b,d] Dongzhi Chi,[a] and Shijie Wang[a,*]*

[a]*Institute of Materials Research and Engineering (IMRE), A*STAR (Agency for Science, Technology and Research), 3, Research Link, Singapore 117602*

[b]*Division of Physics and Applied Physics, School of Physical and Mathematical Sciences, Nanyang Technological University, Singapore 637371*

[c]*School of Material Science and Engineering, Hebei University of Technology, Tianjin 300130, China*

[d]*NOVITAS, Nanoelectronics Centre of Excellence, School of Electrical and Electronic Engineering, Nanyang Technological University, Singapore 639798*

The two-dimensional layer of molybdenum disulfide (MoS_2) exhibits promising prospects in the applications of optoelectronics and valleytronics. Here we report a new successful process to synthesize wafer-scale MoS_2 atomic layers on diverse substrates via magnetron sputtering. Spectroscopic and microscopic results reveal that these synthesized MoS_2 layers are highly homogenous and crystallized. Uniform monolayer at wafer scale can be achieved. The Raman and photoluminescence spectroscopy indicate comparable optical qualities of these as-grown MoS_2 with other methods. The transistors made of the MoS_2 film exhibits *p*-type performance with an on/off current ratio of ~10^3 and hole mobility up to ~12.2 $cm^2\ V^{-1}\ s^{-1}$. The strategy reported here paves new ways towards the large scale growth of various two dimensional semiconductors with the feasibility of controllable doping to realize desired *p*- or *n*-type devices.

*E-mail: jgtao81@gmail.com; jw-chai@imre.a-star.edu.sg; sj-wang@imre.a-star.edu.sg

Introduction

Recently, atomically thin two-dimensional (2D) transition metal dichalcogenides (TMDs), MX_2 (M = Mo, W; X = S, Se, Te), were demonstrated to offer rich collection of physics and functionalities in the area of nanoelectronics,[1-3] optoelectronics,[4] catalysis,[5] photo-detection,[6] photovoltaics[7] and photocatalysis.[8] The lattice of bulk TMDs is formed by covalently bonded X-M-X 2D hexagonal trilayer, which weakly bounds with neighboring layers *via* van der Waals forces.[9, 10] In each layer, the electrons and holes are vertical confined, giving rise to many exotic physics phenomena especially at monolayer limit. When exfoliated down to a monolayer, the band-gap of TMDs crosses over from indirect to direct due to quantum confinement, which entails rather efficient light absorption and emission. As a prototype of TMDs, molybdenum disulfide (MoS_2) has been demonstrated to exhibit high current on/off ratio (1×10^8),[11, 12] high mobility (~200 $cm^2 \cdot V^{-1} s^{-1}$) and negligible off current. This indicates that the sensitivity can be significantly improved with MoS_2-based field effect transistors (FETs).[3, 4, 13] Besides its good electronic properties, the inherent band-gap (1.8 eV for monolayer and 1.2 eV for bulk)[4, 14, 15], excellent mechanical and optical properties avail its applications in large-area flexible optoelectronics.[3] To facilitate the integration of this fascinating material into macroscopic electronic applications, it is essential to develop a large-area growth technique that is compatible with current micro- or nano- fabrication processes.

Single and few-layered MoS_2 were first obtained by top-down mechanical exfoliation technique[11] as commonly used for graphene. Though this exfoliation method has potential to achieve high quality materials, it is not suitable for large scale commercially viable device. More recently, thinning of the TMD few-layers *via* laser,[16] plasma,[17] patterning method[18] or thermal annealing[19] were reported, which require to start with thin layers and hence also lack of large-

scale and massive production feasibility. Later, bottom-up growth methods have been introduced to develop more scalable techniques, including physical vapor deposition (PVD),[20, 21] chemical vapor deposition (CVD),[22, 23] sulfurization of molybdenum oxides,[24] hydrothermal synthesis,[25] and electrochemical lithiation process.[26] Several approaches based on CVD have been reported by using Mo,[27] MoO_3,[23, 24] $MoCl_5$,[22] or $(NH_4)_2MoS_4$[28] as Mo precursor followed by the second-step thermal sulfurization. More recently, seeding promoter has been used to improve the CVD growth quality.[29] Although CVD method has demonstrated its success in synthesis of large scale high quality TMDs on various substrates, the control of thickness, purity and uniformity is still a challenge. For practical application, a scalable and controlled synthesis technique is required. Therefore, alternative approaches, either complementary or advanced, are greatly demanded.

Up to date, the majority of the synthesized MoS_2 films based on abovementioned methods are *n*-type doped.[13, 28, 30] Very recently, it has been reported that *p*-type doped MoS_2 can be realized by efficient plasma treatment.[31] Moreover, the formation of MoS_2 *p-n* junction devices was exhibited by using electric double layer gating.[32, 33] To meet the digital logic application demands, the research for an intrinsically *p*-type TMD monolayer becomes urgent. However, the large-scale device applications still rely on the breakthrough in the growth of large-size controlled doping thin layers.

In this work, we report a one-step process that can grow good quality monolayer or few-layer MoS_2 films at wafer scale on various substrates using magnetron sputtering. The detailed growth procedure is given in the Supporting Information. As is well known, the magnetron sputtering technique is capable of large scale massive production, which is compatible with current industrial process with low cost and easy controllability. Previously, the magnetron sputtering method is barely used for 2D material growth especially for the TMDs. The main

obstacle is possibly the difficulty of controlling of the S or Se sources. In contrast to previous CVD methods,[22-24, 27, 28] the Mo metal was sputtered to produce energized molecular-sized reactive Mo atoms or clusters that are more reactive than Mo or MoO_3 films in the CVD method. The Mo atoms react with vaporized S atoms before landing onto hot substrates to form MoS_2 layers. Our spectroscopic, microscopic and electrical measurements suggest that this synthetic process can lead to the growth of monolayer, bilayer, trilayer and thicker MoS_2 sheets. These MoS_2 films are highly homogeneous and their size is up to several centimeters, which is currently limited by the size of our sample stage. It exhibits optical and electrical qualities comparable to the MoS_2 synthesized by other methods.

Experimental methods

Characterizations: Surface morphology of the samples was examined with commercial atomic force microscope (AFM, Bruker ICON-PKG). Raman spectra were obtained on a single-gating micro-Raman spectrometer (Horiba-JY T64000) excited with 532 nm laser. The signal was collected through a 100× objective, dispersed with a 1800 g/mm grating, and detected by a liquid nitrogen cooled charge-coupled device. Photoluminescence (PL) was obtained from the same micro-Raman spectrometer. The Si peak at 520 cm^{-1} was used for calibration in the experiments.

The samples were *in situ* transferred to an x-ray photoelectron spectroscopy (XPS) chamber for analysis. XPS measurements were performed in a VG ESCALAB 220i-XL system using a monochromatic Al K_α source. The pass energy of the analyzer was set to 10 eV to have high measurement resolution.

Transmission electron microscopy (TEM) (JEOL 2100) was used to obtain information of the microstructures. For sample transfer, poly(methyl methacrylate) (PMMA, from

MicroChem) was spin-coated on top of the sample. After baking at 180 ^{o}C for 2 min, the PMMA coated sample was immersed into 60 ^{o}C 2M NaOH solution to etch the SiO_2 until the PMMA with MoS_2 film floated on the surface. Afterward, a lacey carbon TEM grid was used to fish the PMMA and the MoS_2 film. Finally, the PMMA film was removed by acetone and the MoS_2 layers was cleaned by DI water.

Field-effect transistors fabrication and measurements: To fabricate back-gated MoS_2 FETs, the metallic drain/source contacts (5 nm Cr/100 nm Au) were fabricated by photolithography followed by metal deposition and lift-off. Finally, another Au coating layer was made onto the backside of the Si substrate, which serves as a back gate contact. The device characteristic curves were measured using a Keithley 4200 semiconductor parameter analyzer.

Results and discussion

Figure S1 (see the Supporting Information) schematically illustrates our experimental setup for growing MoS_2. The MoS_2 layers are first grown on *c*-plane sapphire (Al_2O_3) and SiO_2/Si. The as-grown MoS_2 thin films show uniformity and continuity across an area of centimeters under optical microscope or by eyes. Figure 1(a) shows a photograph of MoS_2 thin layer grown on sapphire. The as-grown MoS_2 layer is in faint yellow color and found to have specular reflection without grain boundaries. In addition, the missing of grain boundaries was confirmed via atomic force microscope (AFM) measurement at micrometer scale. Combining these measurements, a large area continuous and uniform MoS_2 film is indicated. The size of the synthesized films is limited by the dimensions of our sample heating holder. The surface morphology is further characterized by AFM at different areas on the film, which exhibit similar surface morphology across the film. A typical AFM measurement (5 μm × 5 μm) is presented in Fig. 1(b), which manifests an atomically flat surface. The AFM images confirm that the

synthesized film possesses a continuous and smooth surface (root-mean-square (RMS) roughness < 0.2 nm) with no step and void observed. The roughness values are comparable to the values for the substrate itself. The thickness variation is found to be negligible, indicating that the films were highly uniform. Similar uniformity can also be achieved for the thicker synthesized MoS_2 films (see Fig. S2 in the Supporting Information). A larger scale AFM image given in Fig. 1(c) shows the edge of the MoS_2 film. In Fig. 1(d), the height profile drawn at the edge reveals the film thickness of ~0.7 nm, which agrees well with one atomic layer of MoS_2.[34] The layer thickness and uniformity assignment are further confirmed by Raman spectroscopy as discussed below.

We controlled the layer thickness via growth parameters, including the deposition time, substrate temperature, growth power etc. To demonstrate the thickness control of the atomically thin MoS_2 layers, Fig. 2 shows the Raman spectra collected from the as-grown MoS_2 thin films on sapphire for variable thickness. The Raman spectra for the MoS_2 films grown on SiO_2 are given in Fig. S3 of supporting information. Comparing the Raman spectra in Fig. 2 and Fig. S3, we found that the MoS_2 film on sapphire exhibits narrower and stronger Raman peak than that on SiO_2, which suggests better crystalline quality of MoS_2 film on sapphire than that on SiO_2/Si. The better crystalline quality of MoS_2 film grown on sapphire is due to the fact that sapphire is atomically flat with step height of 0.22 nm which is sufficiently low to assure the growth of continuous MoS_2 film. In addition, there exist dipole-dipole interactions between S and Al atoms on sapphire which better align the MoS_2 layers.[35] In Fig. S4 of the Supporting Information, the Raman spectra were collected with lower (0.74 mW) and higher (11 mW) laser powers. It is shown that the Raman spectrum under 11 mW laser power exhibits strong signal without burning the sample. Moreover, the peak positions and their separation do not depend on the excitation

laser power, which confirms that there is no laser heating effect. Therefore, 11 mW is used for the following measurements. As shown in Fig. 2a, the MoS_2 films exhibit two Raman characteristic bands at ~406 cm^{-1} and ~386 cm^{-1}, corresponding to out-of-plane (A_{1g}) and in-plane (E^1_{2g}) vibration modes, respectively. The full width at half maximum (FWHM) of the A_{1g} peak of the synthesized MoS_2 monolayer is 4.4 cm^{-1}, close to that of the exfoliated monolayer, 3.7 cm^{-1}, which suggests a good crystalline quality for our synthesized film. As expected, these two bands shift with MoS_2 layer thickness. In addition, the frequency difference (Δk) between A_{1g} and E^1_{2g} modes has been used to identify the layer number of MoS_2. In general, the E^1_{2g} vibration softened, whereas the A_{1g} vibration stiffened at higher layer number. This is demonstrated in Fig. 2(a) that the A_{1g} is blue-shifted and E^1_{2g} is red-shifted with the increase of film thickness. The Δk of the synthesized thin film increases from 19.3 to 24.3 cm^{-1} from monolayer to bulk. The assignment of Δk = 19.3 cm^{-1} to monolayer is in agreement with previous reports.[22, 27, 36] The thickness of bilayer (2L) and trilayer (3L) is confirmed by transmission electron microscope (TEM) measurement as presented below. Note that the optimized process reported here is fairly easy to reproduce homogeneous MoS_2 bilayer or trilayer. However, the monolayer MoS_2 is more difficult to achieve, which is attributed to the growth kinetics of this process.

The uniformity of the layers is quantitatively assessed by conducting numerous Raman spectra at random spots over a typical ~1 cm × 1 cm sapphire substrate. Figure 2(b) shows Raman spectra for each measured spot for a monolayer MoS_2. It is known that the peak width of the Raman peak is also sensitive to the crystalline quality and therefore the FWHMs of all E^1_{2g} and A_{1g} modes are also analyzed. As shown in Fig. 2(b), the variation of Δk and FWHMs are reasonably small, ±0.27 cm^{-1} for Δk and ±0.16 cm^{-1} for FWHMs, respectively. These results

confirm that the synthesis method described here can provide highly homogeneous films with similar crystalline quality across the entire substrate. In addition, shear or breathing Raman modes would appear at low frequency for multi-layers.[36, 37] The absence of these modes cross over the surface of our sample suggests the formation of uniform monolayer in large scale.

X-ray photoemission spectroscopy (XPS) was used to examine the film-substrate interface chemistry as well as the electronic structure of the synthesized films. Figure 3 shows the core-level XPS spectra of Mo 3*d*, S 2*p* and valence band (VB) for MoS_2 films on sapphire. The peaks at 229.3 and 232.5 eV are attributed to the doublet Mo $3d_{5/2}$ and $3d_{3/2}$ orbitals, respectively, in agreement with reported binding energy values.[26, 28] Thermodynamics point of view, Mo layer would prefer to bind to oxide surface to form an interfacial Mo-O oxide on an oxidized substrate. However, our XPS analysis shows no evidence of Mo-O peak at higher energy side suggests a negligible interfacial interaction, owing to kinetics reasons. As shown in Fig. 3(b), the spin-orbital splitting for S 2*p* is well resolved into S $2p_{3/2}$ and $2p_{1/2}$ at 162.2 and 163.3 eV, respectively. Especially, the S 2*p* spectrum of the 2L film almost bears the same shape of the bulk one, which implies good crystalline structure for the atomically thin film. In addition, as demonstrated before, 1T-MoS_2 and 2H-MoS_2 phases display distinguished binding energies for Mo 3*d*.[26] Our XPS results support the formation of pure phase of 2H-MoS_2 crystal structure. The valence band of MoS_2 is built up by the hybridization of Mo 4*d* and S 3*p*, which exhibits four major features within 0~10 eV.[38] As shown in Fig. 3(c), the electronic states of Mo $4d_{z^2}$ band is readily developed at ~2 eV[38] for monolayer MoS_2. The higher binding energy Mo 4*d* - *S* 3*p* orbitals are overlapped with the substrate O 2*p* peaks and are gradually pronounced with increasing the layer thickness. These observations indicate well-developed bands formation from hybridized Mo 4*d* - *S* 3*p* orbitals, which imply long-range in-plane ordering of the MoS_2

structure. Along with development of the valence band structure, the separation between the Mo $3d_{5/2}$ and Mo $4d_{z^2}$ peaks increases with the layer thicknesses, see Fig. S5 of the Supporting Information. It changes from 227.25 eV for monolayer to 227.55 eV for thicker films. This observation confirms the development of electronic structure of MoS_2 film with the thickness as demonstrated before.[39] In addition, the smaller separation for the monolayer implies a better screening effect of the valence electrons to the core level. Our synthesized thick film shows almost identical XPS spectra to that of commercial bulk sample, as shown in Fig. S6 of supporting information, indicating good quality synthesized film can be obtained using our novel large area one-step sputtering process.

To further elucidate the crystalline structure, the as-grown MoS_2 film was transferred onto a lacey carbon grid for TEM characterization. A typical high resolution TEM image as well as the selected area electron diffraction (SAED) pattern are given in Fig. 4(a), which reveals the ordered crystalline with hexagonal lattice structure and the lattice spacing of 0.27 nm for (100) planes is observed. The hexagonal atomic arrangement shown in the TEM image and the SAED pattern indicate that the basal plane of the synthesized thin film is (001), *i.e.* the c-axis of the MoS_2 films is perpendicular to the substrate. Figure 4(b) is the magnified TEM image for the area squared by the black solid lines in Fig. 4(a). The periodic atom arrangement for Mo is given, inferring that the MoS_2 film forms crystalline structure. The MoS_2 film on TEM grids exhibit some wrinkles on the edge of the film, which is caused by unavoidable film folding of the free-hanging MoS_2 sheets at the edge during the TEM sample preparation. This, however, permit the assessment of layer number under top-view TEM. For instance, bilayer (2L) and trilayer (3L) edges are displayed in Fig. 4(c). This local layer thickness characterization is in line with the Raman spectra mentioned above.

In addition, photoluminescence (PL) measurement at room temperature is shown in Fig. 4(d), exhibiting the layer dependent optical properties. The PL spectrum for the monolayer MoS_2 exhibits the strongest emission at 1.83 eV as well as a shoulder at 2.00 eV, which can be correlated to the A and B exciton transition arising from direct gap transitions at the *K* point. These excitonic energies as well as the splitting of ~170 meV agree well with previous reports,[4, 14, 26] which is resulted from the strong spin-orbit coupling due to the breaking of inversion symmetry.[40, 41] The PL response confirms the direct band transition in 2H-MoS_2 monolayer. Our results suggest a comparable optical quality as other synthesized MoS_2 films.[28, 42] The strong PL intensity for monolayer MoS_2 is dramatically dropped for bilayer film and falls to zero when the layer number is larger than three. This suggests that the band structure of our MoS_2 film bears a similar dependence with that of exfoliated films, thus further confirm the layer number assignment for our sputtering-grown MoS_2 films. We note that, similar to some of previous reports,[43, 44] the exciton B peak is less resolved as compared to the mechanically exfoliated monolayer. This could be due to the presence of lattice disorder or residual dopants that decouple the spin-orbital interaction.

Thin layers MoS_2 are well suited as a channel material in field effect transistor (FET) applications exhibiting high mobility, almost ideal switching characteristic and low standby power dissipation. To evaluate the electrical performance of the as-grown MoS_2 sheets, we fabricated bottom-gate FETs on MoS_2 films by evaporating Cr/Au electrodes as source and drain electrodes on top of the MoS_2 thin film, 200 nm thick SiO_2 as dielectrics and Au coated Si as back gate. We performed electrical measurements at room temperature in an ambient environment. Figure 5(a) shows the typical transport characteristic of a representative device having a channel length of 100 μm and width of 10 μm as shown in the inset. In contrast to

previous results,[13, 28, 30] a *p*-type field effect behavior is exhibited with an on/off current ratio of ~10^3 at ~ -20 V gate voltage (V_g) and bias voltage (V_{ds}) at 4 V. The linear dependence of drain current (I_{ds}) –V_{ds} characteristic curves, see Fig. 5(b), suggests ohmic contact between the film and electrodes. This warrants that the observed field effect behavior is from the MoS_2 channel rather than Schottky barriers at the contact. Consistent with the transfer curves, the I_{ds} increases at negative gate voltage, indicating that the hole is the majority carrier. From the measurements, the value of hole field-effect mobility (μ) of *this* MoS_2 FET is estimated to be ~12.2 $cm^2 \cdot V^{-1} s^{-1}$ based on the slop of $\frac{\Delta I_{ds}}{\Delta V_g}$ fitted to the linear regime of the transfer curves using the expression,

$$\mu = \left(\frac{LC_{ox}V_d}{W}\right)\left(\frac{\Delta I_{ds}}{\Delta V_g}\right) \quad (1)$$

where L and W is the length and width of the channel, respectively, C_{ox} is the capacitance between the channel and the back-gate per unit area (~1.7×10^{-4} F m^{-2} for 200 nm SiO_2). We have performed many measurements over several channels, and found the mobility ranging from ~ 2 to ~12 $cm^2 \cdot V^{-1} s^{-1}$ which is centered at ~7 $cm^2 \cdot V^{-1} s^{-1}$. This result is reasonably comparable to those of back-gated FETs made with mechanically exfoliated monolayers measured in similar conditions (0.1−10 $cm^2 \cdot V^{-1} s^{-1}$).[13, 23, 24, 27, 28] The mobility of the MoS_2 FETs could be significantly improved by using local top-gate high-κ dielectric, such as HfO_2, as gate materials. We can thus conclude that the synthesized thin film has a reasonably comparable electrical quality with exfoliated MoS_2. We speculate that by controlling annealing time, annealing environment or the substrate material, the film quality can be further improved, leading to higher carrier mobility.

The *p*-type doping could be originated from cationic/anionic vacancies/interstitials that are introduced during the deposition process. Tentatively, this is assigned to the S interstitials based on slightly larger S concentration from our XPS measurement (atomic ratio of Mo:S ~

1:2.06). In addition, recent theoretical calculations predict that the absorption of H_2, O_2, and H_2O on the surface of MoS_2 can also result in *p*-type doping.[45] This could mostly happen at the surface defect sites.

The major difference between our one-step sputtering growth method and other growth methods, such as CVD, is the kinetic energy of landing MoS_2 molecules. The typical kinetic energies of landing molecules are on the order of tens eV even after multiple scattering events within the background gas. This residual energy warrants the in-plane movement. With this energy, the requirement for the nucleation center as required for CVD growth[34] is no longer a key issue. Our experimental observations suggest that the Ar pressure and sputtering power play key roles in this growth mechanism. With this difference, different crystal structure imperfection may be introduced as compared to previous methods. This, however, brings new functionalities and opens new possibilities to explore the material properties. In case of CVD growth, S vacancies are normally formed that leads to *n*-type doping. While using sputtering method, additional energized S can be incorporated into the lattice to serve as *p*-type dopants, which is the case as we demonstrated here. Note that the S interstitials is not observed for CVD film, suggesting the excess S vapor itself is not enough to warrant *p*-type doping, but the sufficient kinetic energy. Under Mo deficiency conditions, either Mo vacancies or S interstitials will create acceptor level inside the band gap of MoS_2 that leads to *p*-type doping. Although the detailed growth dynamics studies require further investigations, which are not covered by current work, we note that the doping type can be modulated via the sputtering power and the *p*-type doping is related to the Mo deficiency conditions. Moreover, we like to emphasize that the controlled doping study can be easily realized via using some alloy targets adopting this strategy.

Conclusion

In conclusion, we demonstrated a proof-of-concept one-step large-area synthesis of uniform MoS_2 films with readily control over the layer number using magnetron sputtering method. This method can be used to produce large-area, good quality MoS_2 monolayer and few-layer films with great uniformity and controllability. The electric measurement for the bottom-gate transistor shows *p*-type semiconductor behavior. The on/off current ratio is ~1×10^3 and the hole mobility is up to ~12.2 $cm^2 \cdot V^{-1} s^{-1}$. This synthesis approach can be readily scaled up to produce wafer-scale 2D MoS_2 for the development of practical electronic and photonic devices. This synthesis method could be extended to the growth of other TMDs as well as controlled doping for these systems, opening up new avenues for the 2D material studies.

References:

1. K. S. Novoselov, D. Jiang, F. Schedin, T. J. Booth, V. V. Khotkevich, S. V. Morozov and A. K. Geim, *PNAS*, 2005, **102**, 10451-10453.
2. C. Lee, Q. Li, W. Kalb, X.-Z. Liu, H. Berger, R. W. Carpick and J. Hone, *Science*, 2010, **328**, 76-80.
3. Q. H. Wang, K. Kalantar-Zadeh, A. Kis, J. N. Coleman and M. S. Strano, *Nat Nano.*, 2012, **7**, 699-712.
4. K. F. Mak, C. Lee, J. Hone, J. Shan and T. F. Heinz, *Phys. Rev. Lett.*, 2010, **105**, 136805.
5. K. H. Hu, X. G. Hu and X. J. Sun, *Appl. Surf. Sci*, 2010, **256**, 2517-2523.
6. Z. Yin, H. Li, H. Li, L. Jiang, Y. Shi, Y. Sun, G. Lu, Q. Zhang, X. Chen and H. Zhang, *ACS Nano*, 2012, **6**, 74-80.
7. E. Gourmelon, O. Lignier, H. Hadouda, G. Couturier, J. C. Bernède, J. Tedd, J. Pouzet and J. Salardenne, *Sol. Energy Mater. Sol. Cells*, 1997, **46**, 115-121.
8. W. Ho, J. C. Yu, J. Lin, J. Yu and P. Li, *Langmuir*, 2004, **20**, 5865-5869.
9. R. A. Bromley, R. B. Murray and A. D. Yoffe, *J. Phys. C*, 1972, **5**, 759.
10. L. F. Mattheiss, *Phys. Rev. B*, 1973, **8**, 3719-3740.
11. RadisavljevicB, RadenovicA, BrivioJ, GiacomettiV and KisA, *Nat Nano.*, 2011, **6**, 147-150.
12. L. Ming-Wei, L. Lezhang, L. Qing, T. Xuebin, S. D. Kulwinder, Z. Peng, M. N. Vaman, C. Mark Ming-Cheng and Z. Zhixian, *J. Phys. D: Appl. Phys.*, 2012, **45**, 345102.
13. B. Radisavljevic, A. Radenovic, J. Brivio, V. Giacometti and A. Kis, *Nat Nano.*, 2011, **6**, 147-150.
14. A. Splendiani, L. Sun, Y. Zhang, T. Li, J. Kim, C.-Y. Chim, G. Galli and F. Wang, *Nano Lett.*, 2010, **10**, 1271-1275.
15. S. Lebègue and O. Eriksson, *Phys. Rev. B*, 2009, **79**, 115409.
16. A. Castellanos-Gomez, M. Barkelid, A. M. Goossens, V. E. Calado, H. S. J. van der Zant and G. A. Steele, *Nano Lett.*, 2012, **12**, 3187-3192.
17. Y. Liu, H. Nan, X. Wu, W. Pan, W. Wang, J. Bai, W. Zhao, L. Sun, X. Wang and Z. Ni, *ACS Nano*, 2013, **7**, 4202-4209.
18. M. I. B. Utama, X. Lu, D. Zhan, S. T. Ha, Y. Yuan, Z. Shen and Q. Xiong, *Nanoscale*, 2014.

19. X. Lu, M. I. B. Utama, J. Zhang, Y. Zhao and Q. Xiong, *Nanoscale*, 2013, **5**, 8904-8908.
20. S. Helveg, J. V. Lauritsen, E. Lægsgaard, I. Stensgaard, J. K. Nørskov, B. S. Clausen, H. Topsøe and F. Besenbacher, *Phys. Rev. Lett.*, 2000, **84**, 951-954.
21. J. V. Lauritsen, J. Kibsgaard, S. Helveg, H. Topsoe, B. S. Clausen, E. Laegsgaard and F. Besenbacher, *Nat Nano.*, 2007, **2**, 53-58.
22. Y. Yu, C. Li, Y. Liu, L. Su, Y. Zhang and L. Cao, *Sci. Rep.*, 2013, **3**, 1866.
23. Y.-H. Lee, X.-Q. Zhang, W. Zhang, M.-T. Chang, C.-T. Lin, K.-D. Chang, Y.-C. Yu, J. T.-W. Wang, C.-S. Chang, L.-J. Li and T.-W. Lin, *Adv. Mater.*, 2012, **24**, 2320-2325.
24. Y.-C. Lin, W. Zhang, J.-K. Huang, K.-K. Liu, Y.-H. Lee, C.-T. Liang, C.-W. Chu and L.-J. Li, *Nanoscale*, 2012, **4**, 6637-6641.
25. Y. Peng, Z. Meng, C. Zhong, J. Lu, W. Yu, Y. Jia and Y. Qian, *Chem. Lett.*, 2001, **30**, 772-773.
26. G. Eda, H. Yamaguchi, D. Voiry, T. Fujita, M. Chen and M. Chhowalla, *Nano Lett.*, 2011, **11**, 5111-5116.
27. Y. Zhan, Z. Liu, S. Najmaei, P. M. Ajayan and J. Lou, *Small*, 2012, **8**, 966-971.
28. K.-K. Liu, W. Zhang, Y.-H. Lee, Y.-C. Lin, M.-T. Chang, C. Su, C.-S. Chang, H. Li, Y. Shi, H. Zhang, C.-S. Lai and L.-J. Li, *Nano Lett.*, 2012, **12**, 1538-1544.
29. X. Ling, Y.-H. Lee, Y. Lin, W. Fang, L. Yu, M. S. Dresselhaus and J. Kong, *Nano Lett.*, 2014, **14**, 464-472.
30. H. Li, Z. Yin, Q. He, H. Li, X. Huang, G. Lu, D. Fam, A. Tok, Q. Zhang and H. Zhang, *Small*, 2012, **8**, 63 - 67.
31. H. Nam, S. Wi, H. Rokni, M. Chen, G. Priessnitz, W. Lu and X. Liang, *ACS Nano*, 2013, **7**, 5870-5881.
32. Y. J. Zhang, J. T. Ye, Y. Yomogida, T. Takenobu and Y. Iwasa, *Nano Lett.*, 2013, **13**, 3023-3028.
33. Y. Zhang, J. Ye, Y. Matsuhashi and Y. Iwasa, *Nano Lett.*, 2012, **12**, 1136-1140.
34. S. Najmaei, Z. Liu, W. Zhou, X. Zou, G. Shi, S. Lei, B. I. Yakobson, J.-C. Idrobo, P. M. Ajayan and J. Lou, *Nat. Mater.*, 2013, **12**, 754-759.
35. D. Dumcenco, D. Ovchinnikov, K. Marinov, O. Lopez-Sanchez, D. Krasnozhon, M.-W. Chen, P. Gillet, A. F. i. Morral, A. Radenovic and A. Kis, *arXiv:1405.0129v1* 2014.

36. Y. Zhao, X. Luo, H. Li, J. Zhang, P. T. Araujo, C. K. Gan, J. Wu, H. Zhang, S. Y. Quek, M. S. Dresselhaus and Q. Xiong, *Nano Lett.*, 2013, **13**, 1007-1015.

37. X. Zhang, W. P. Han, J. B. Wu, S. Milana, Y. Lu, Q. Q. Li, A. C. Ferrari and P. H. Tan, *Phys. Rev. B*, 2013, **87**, 115413.

38. K. S. Liang, G. J. Hughes and R. R. Chianelli, *J. Vac. Sci. Technol. A* 1984, **2**, 991-994.

39. W. Jin, P.-C. Yeh, N. Zaki, D. Zhang, J. T. Sadowski, A. Al-Mahboob, A. M. van der Zande, D. A. Chenet, J. I. Dadap, I. P. Herman, P. Sutter, J. Hone and R. M. Osgood, *Phys. Rev. Lett.*, 2013, **111**, 106801.

40. SuzukiR, SakanoM, Y. J. Zhang, AkashiR, MorikawaD, HarasawaA, YajiK, KurodaK, MiyamotoK, OkudaT, IshizakaK, AritaR and IwasaY, *Nat Nano*, 2014, **9**, 611-617.

41. N. Alidoust, G. Bian, S.-Y. Xu, R. Sankar, M. Neupane, C. Liu, I. Belopolski, D.-X. Qu, J. D. Denlinger, F.-C. Chou and M. Z. Hasan, *Nat. Commun.*, 2014, **5**.

42. Y. Lee, J. Lee, H. Bark, I.-K. Oh, G. H. Ryu, Z. Lee, H. Kim, J. H. Cho, J.-H. Ahn and C. Lee, *Nanoscale*, 2014, **6**, 2821-2826.

43. A. P. S. Gaur, S. Sahoo, M. Ahmadi, S. P. Dash, M. J. F. Guinel and R. S. Katiyar, *Nano Lett.*, 2014, **14**, 4314-4321.

44. K. Mak, C. Lee, J. Hone, J. Shan and T. Heinz, *Phys. Rev. Lett.*, 2010, **105**, 136805.

45. Q. Yue, Z. Shao, S. Chang and J. Li, *Nanoscale Res. Lett.* , 2013, **8**, 425.

Figure captions:

Fig. 1. **Large-area uniform MoS_2 films on sapphire substrate.** (a) Photograph of a MoS_2 film on sapphire substrate. (b) AFM image of the as-growth MoS_2 film. (c) A larger scanning area AFM image of the as-growth film with clear edge of film. (d) Height profile from section as indicated by the blue line in panel (c). The monolayer MoS_2 is ~ 0.7 nm in thickness.

Fig. 2. **Raman spectra of the as-grown MoS_2 on sapphire.** (a) Development of the Raman spectra for monolayer (1L), bilayer (2L), trilayer (3L) and thick (bulk) MoS_2 sample. The two characteristic Raman modes are labeled. The small peak at ~418 cm^{-1} is originated from sapphire substrate. The dashed vertical lines indicate the peak positions for monolayer sample. (b) Raman spectra collected from 8 random spots of the MoS_2 monolayer film. All the measured frequency separation (Δk) is 19.3 cm^{-1}.

Fig. 3. **Normalized XPS spectra of as-grown MoS_2 on sapphire.** (a) Mo 3*d* (b) S 2*p* spectra and (c) valence band (VB) as a function of the film thickness: monolayer (1L, black curves), bilayer (2L, red curves), trilayer (3L, blue curves) and thick (bulk, pink curves) MoS_2 sample.

Fig. 4. **Crystal structure characterization of the MoS_2 film using TEM.** (a) High resolution TEM image of the MoS_2 film transferred on lacey carbon grid. The inset shows the diffraction pattern of the electron-transmitting area showing the hexagonal symmetry of the MoS_2 structure. (b) Zoom-in image of the area highlighted in (a). The hexagonal structure formed by Mo atoms is indicated. (c) TEM image at the folded area at the edge from a bilayer (2L) and trilayer (3L) samples. All scale bars in (a)-(c) are 2 nm. (d) Thickness dependent photoluminescence spectra

of MoS_2 films on SiO_2. Layer numbers are indicated on the curves. The inset of (d) is a zoom-in image to highlight the existence of B excition transition.

Fig. 5. **Electrical properties of the MoS_2 films on SiO_2/Si.** (a) Transfer curves: $I_{ds} - V_g$ curves plotted in semilog (black curve) and linear (pink curve) scale at V_{ds} = 4 V. Inset: optical image of the back-gated FET device. (b) Output characteristics: $I_{ds} - V_{ds}$ curves of the device for various positive and negative gate voltages. Inset: optical image of the device array.

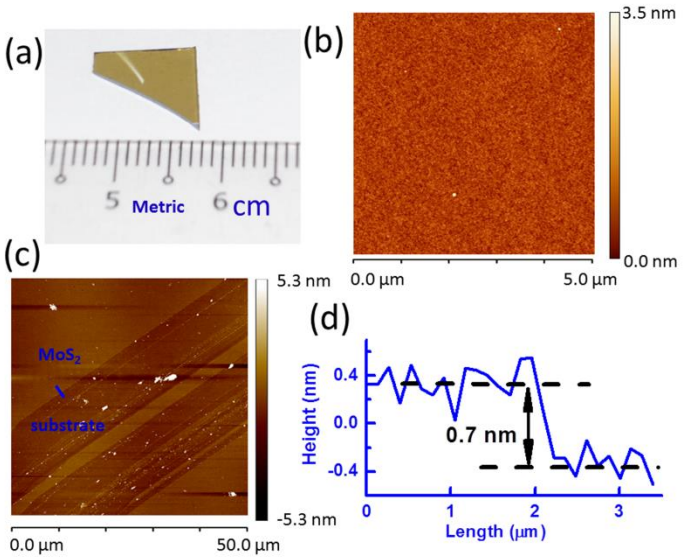

Fig. 1 Tao *et. al.*

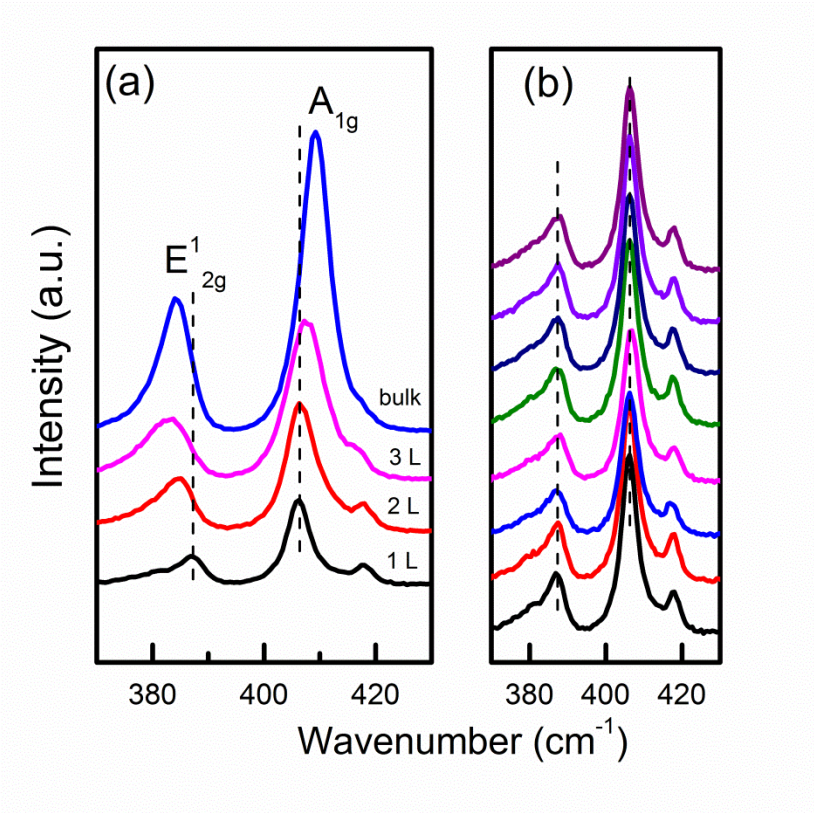

Fig. 2 Tao *et. al.*

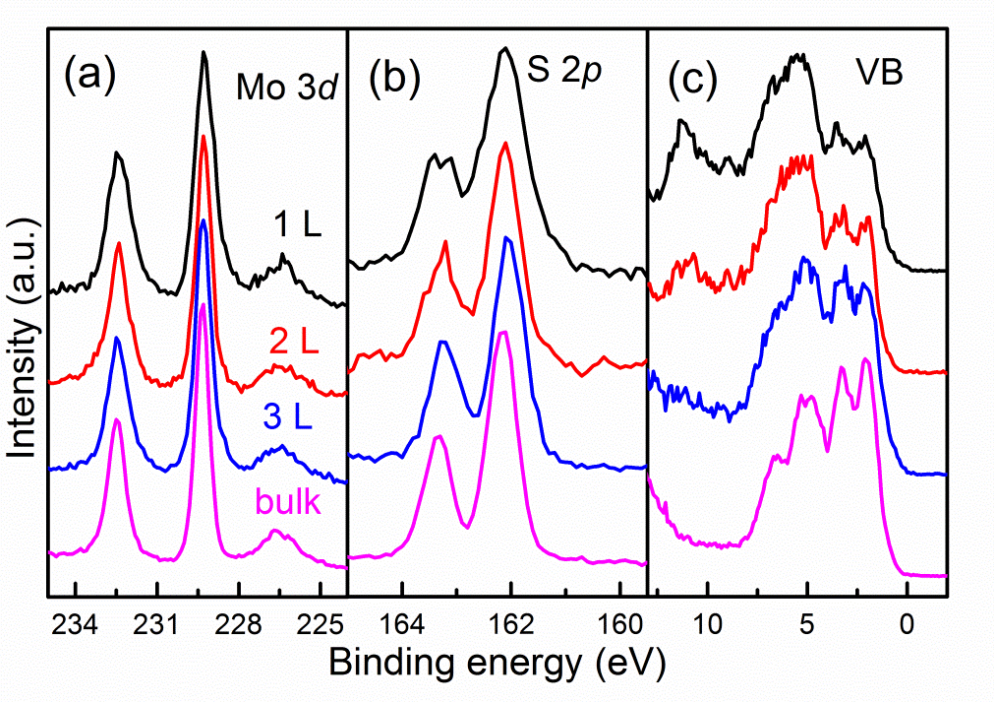

Fig. 3 Tao *et. al.*

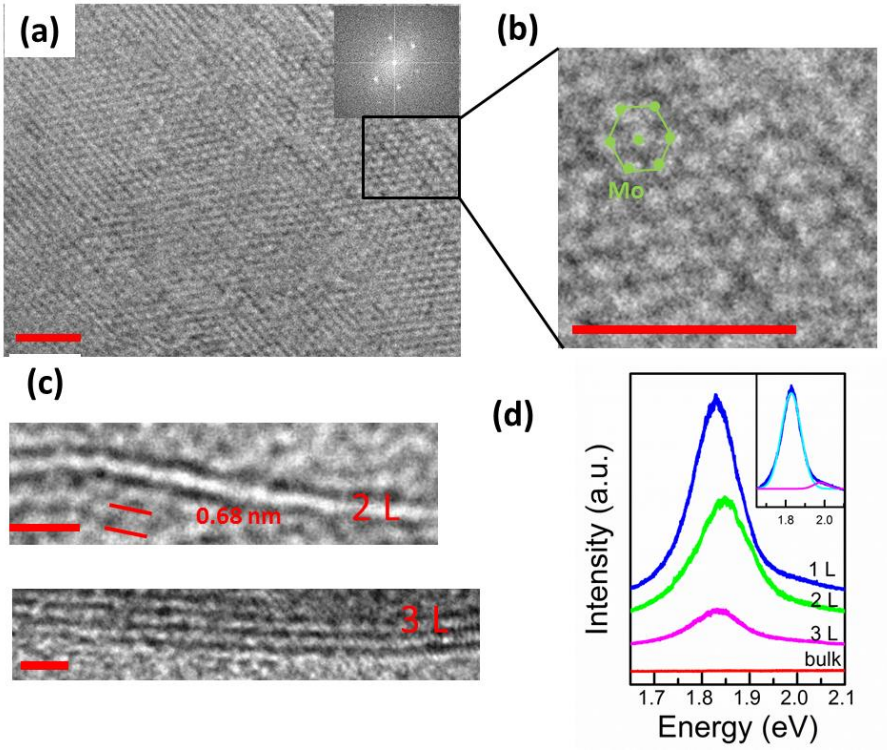

Fig. 4 Tao *et. al.*

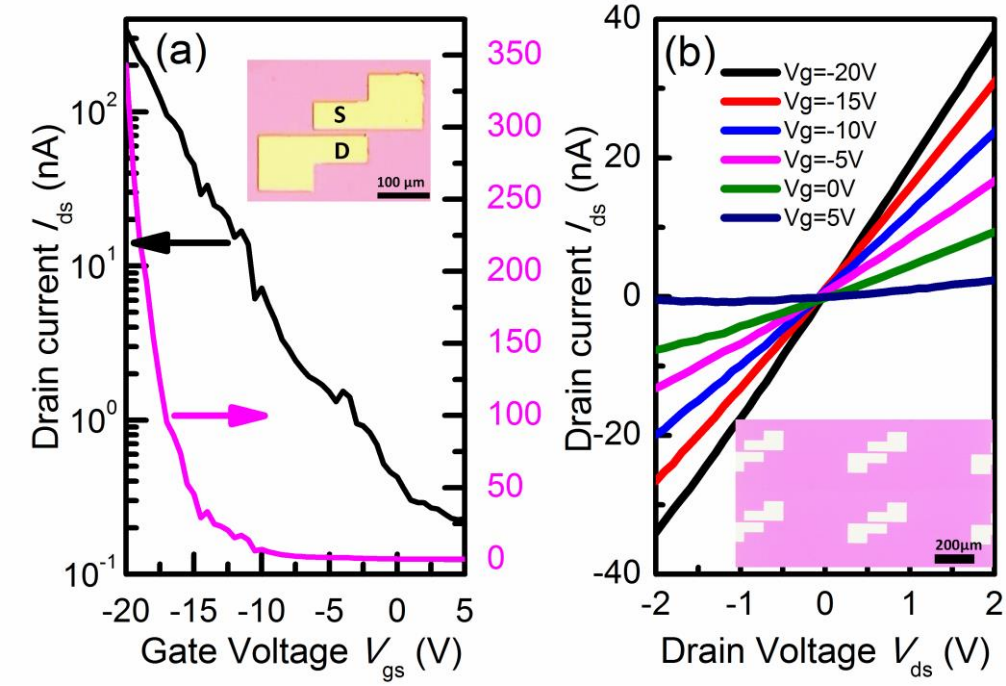

Fig. 5 Tao *et. al.*